Miniaturized 28-GHz Packaged Bandpass Filter With High Selectivity and Wide Stopband Using Multilayer PCB Technology

Yunbo Rao, *Graduate Student Member, IEEE*, Huizhen Jenny Qian, *Member, IEEE*, Jie Zhou, *Student Member, IEEE*, Yuandan Dong, *Senior Member, IEEE*, and Xun Luo, *Senior Member, IEEE*

***Abstract*— In this letter, a packaged bandpass filter (BPF) with a compact size of 1.5 × 1.5 × 0.315 mm^3 operating at 28 GHz is proposed. This BPF is implemented based on a multilayers printed circuit board (PCB) fabrication process with ultra-thin substrate. With the packaged configuration, the filter can not only reduce the circuit size and component insertion loss, but also eliminate the effect of electromagnetic (EM) radiation. To verify the mechanisms mentioned above, a packaged millimeter-wave (mm-wave) BPF with three transmission zeros is designed and fabricated. The measured results show that the proposed BPF has the merits of low insertion loss, high selectivity, and compact size. Meanwhile, this BPF can suppress harmonics with a rejection level of more than 24 dB up to 110 GHz. With these merits, the proposed BPF is attractive for 5G mm-wave application.**

***Index Terms*— 5G, bandpass filter (BPF), high selectivity, millimeter-wave (mm-wave), wide stopband.**

I. Introduction

With ever-increasing demands of wireless communication systems, high performance bandpass filters (BPFs) are essential to 5G applications including sub-6-GHz and millimeter-wave (mm-wave). The BPFs using stepped-impedance resonator (SIR) [1]–[3], defected ground structure (DGS) [4]–[7], and substrate-integrated DGS (SIDGS) [8]–[11] are reported with low loss and wide stopband for sub-6-GHz application. To satisfy the requirements of 5G mm-wave system, the cavity [12]–[16] and substrate-integrated waveguide (SIW) [17]–[21] are used for BPF with good in-band performance. However, the relatively large circuit size cannot integrate for 5G wireless applications (e.g., mobile phone). To reduce the circuit size, on-chip mm-wave BPFs [22]–[30] are introduced, while the relatively poor passband/stopband performance and high fabrication cost limit the applications. Recently, the semiadditive patterning process [31] and low temperature co-fired ceramic (LTCC) technology [32]–[36] are utilized for BPF designs. Nevertheless, these BPFs are not easy to integrate with antenna, power supply, and chip in a packaged micro-system. Therefore, the design of 5G mm-wave BPF with merits of low loss, compact size, low cost, and easy for integration remains great challenges.

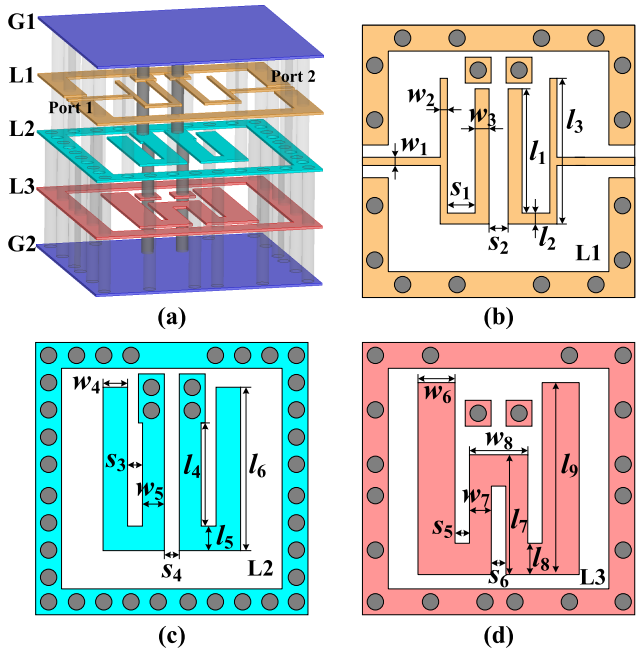

Fig. 1. Configuration of the proposed packaged BPF. (a) 3-D view. (b) Top view of layer L1. (c) Top view of layer L2. (d) Top view of layer L3.

In this letter, a compact BPF with high selectivity and wide stopband is proposed for 5G mm-wave applications. It is fabricated by a commercially five-layer PCB technology. Three controllable transmission zeros are allocated based on the proposed coupling topology to improve passband selectivity. Meanwhile, U-shape resonators and feed lines are stacked up to minimize the circuit size. To verify the mechanism mentioned above, a prototype BPF operating at 28 GHz is implemented and fabricated. The measured results show that the proposed BPF has advantages of low insertion loss, high selectivity, wide stopband, compact size, and easy to integrate.

II. Schematic and Operation

The 3-D-view configuration of the proposed filter is shown in Fig. 1(a). The material (i.e., Panasonic, Megtron 7) is selected as the substrate. The loss tangent is 0.013, which is obtained from the measured results with the sample thickness

Manuscript received February 28, 2022; accepted March 21, 2022. Date of publication April 13, 2022; date of current version June 7, 2022. This work was supported by the National Natural Science Foundation of China (NSFC) under Grant 61934001 and Grant 62161160310. *(Corresponding author: Xun Luo.)*

The authors are with the Center for Advanced Semiconductor and Integrated Micro-System, University of Electronic Science and Technology of China, Chengdu 611731, China (e-mail: xun-luo@ieee.org).

This article was presented at the IEEE MTT-S International Microwave Symposium (IMS 2022), Denver, CO, USA, June 19–24, 2022.

Color versions of one or more figures in this letter are available at https://doi.org/10.1109/LMWC.2022.3163613.

Digital Object Identifier 10.1109/LMWC.2022.3163613

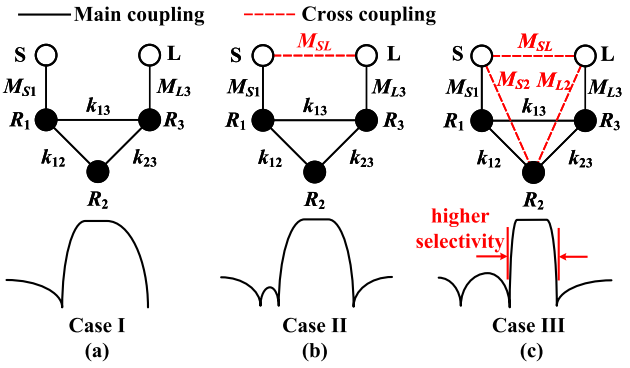

Fig. 2. (a) Traditional CT-type coupling topology. (b) CT-type coupling topology with source/load coupling. (c) Proposed coupling topology.

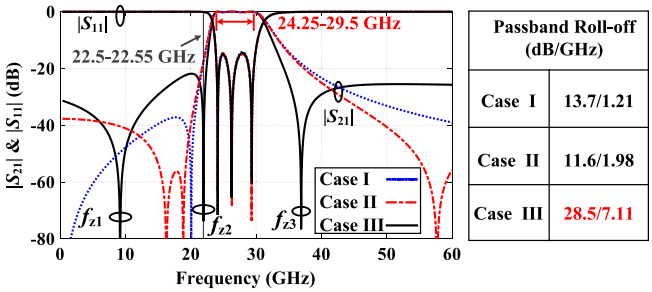

Passband Roll-off (dB/GHz)	
Case I	13.7/1.21
Case II	11.6/1.98
Case III	28.5/7.11

Fig. 3. Calculated S-parameters with different coupling topologies (i.e., Case I–III).

of 0.06 mm at 60 GHz. Besides, the thicknesses of each metal and dielectric layers are 15 and 60 μm, respectively. As shown in Fig. 1(b)–(d), two U-shape feed-lines and three packaged stripline resonators are placed at middle three layers (i.e., layer L1–L3), respectively. To verify the mechanism, the electromagnetic (EM) simulator high frequency structure simulator (HFSS) are used.

A. Coupling Topology for High Selectivity

In this section, a low-order filter with high selectivity is discussed. First, the coupling topology of traditional CT-type is introduced in Fig. 2(a). It can allocate a transmission zero at the lower passband. However, the passband selectivity is relatively low. As shown in Fig. 2(b), the passband selectively is improved once the source/load coupling is introduced, since two additional transmission zeros are allocated at both sides of the passband. To further improve the passband selectivity, a novel cross coupling between source/load and resonator R_2 is added, as depicted in Fig. 2(c). The positions of transmission zeros can be finely adjusted by the coupling strength of $M_{S2/L2}$, which can further improve the passband selectivity. Based on the proposed coupling topology, the design coupling matrix $[M]$ can be obtained by the method in [37]. The calculated S-parameters between different coupling topologies (i.e., Case I–III in Fig. 2) are compared in Fig. 3. The proposed coupling topology can allocate three transmission zeros (i.e., f_{z1}, f_{z2}, and f_{z3}) to effectively improve passband selectivity. Meanwhile, the calculated S-parameters of transmission zeros with different M_{SL} and $M_{S2/L2}$ are depicted in Fig. 4(a) and (b), respectively. The positions of transmission zeros can be finely adjusted by M_{SL} and $M_{S2/L2}$.

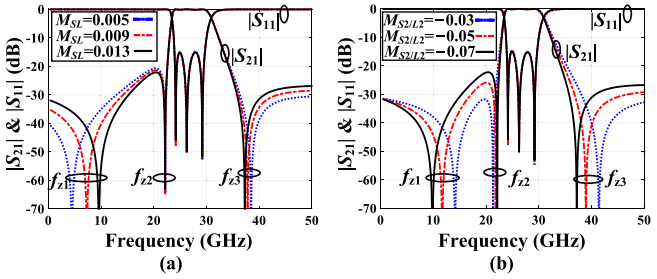

Fig. 4. (a) Variation of transmission zeros with different M_{SL}. (b) Variation of transmission zeros with different $M_{S2/L2}$.

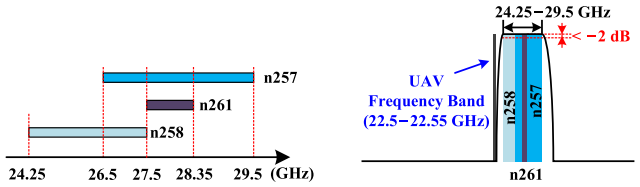

Fig. 5. 5G mm-wave frequency band and design specifications of proposed filter.

B. Filter Design

To meet the requirements of 5G mm-wave bands (i.e., n258, n257, and n261, as shown in Fig. 5), the proposed BPF is set to support three mm-wave frequency bands, simultaneously. Besides, the frequency band (i.e., 22.5–22.55 GHz) is used for control and non-payload communications (CNPCs) of unmanned aerial vehicle (UAV) in Rep-ITU-R [38], which should be suppressed with a high rejection level. Therefore, a prototype of mm-wave packaged BPF is proposed with the following design specifications: passband of 24.25–29.5 GHz, insertion loss lower than 2 dB, return loss higher than 15 dB, and $|S_{21}|$ lower than -25 dB from 22.5 to 22.55 GHz.

To achieve the specifications based on the proposed coupling topology, two grounded $\lambda/4$ stripline resonators (i.e., R_1 and R_3) and one $\lambda/2$ stripline resonator (i.e., R_2) are utilized. Meanwhile, the unloaded Q of grounded $\lambda/4$ resonators and $\lambda/2$ resonator are 102 and 94 (i.e., simulated by HFSS) in filter implementation, respectively. Two U-shape striplines act as the feed-line. The configurations are shown in Fig. 1, which are placed at layer L1–L3, respectively. As shown in Fig. 6(a) and (b), the main couplings (i.e., $M_{S1/L3}$ and $k_{12/23}$) are achieved by top-bottom coupling scheme. The k_{13} is the different coupling type in CT-type filter design, which is implemented by two coupled grounded $\lambda/4$ resonators in Fig. 6(c). The edge-coupled scheme is used to generate source/load coupling (i.e., M_{SL}) between two feed-lines, as depicted in Fig. 6(d). Then, the cross coupling $M_{S2/L2}$ is achieved by cross-layer coupling in Fig. 6(e). Therefore, the configuration of core circuit is shown in Fig. 6(f). Besides, the grounded $\lambda/4$ resonators and $\lambda/2$ resonator have different harmonic distribution due to the stepped-impedance configuration. Thus, a wide stopband response can be achieved by mutual suppression of harmonics [39]. The values of coupling coefficients k_{ij} between two coupled resonators can be extracted by the method in [40]. To achieve the desired couplings coefficients, the design curves of Q_e against l_3 are shown in Fig. 7(a). Besides, the

TABLE I
COMPARISON OF THE REPORTED mm-WAVE BPF WITH STATE-OF-THE-ARTS

Ref.	Technology	Unloaded Q	f_0 (GHz)	FBW (%)	Roll-off (dB/GHz)	IL** (dB)	RL*** (dB)	Lower stopband suprression	Upper stopband suppression	Stopband bandwidth	Size (mm^3)
[13]	HRSi thin-film	166	60	6	4.25/3.95*	1.5	>20	<–20 dB DC to 55 GHz*	<–20 dB 66 to 93 GHz*	$1.55f_0$*	2.38×2.33×1.7
[18]	Single-layer PCB	195	32.8	18.3	4.48/23.7*	1.55	>12	<–20 dB 20 to 27 GHz*	<–20 dB 36 to 41 GHz*	$1.25f_0$*	7.86×7.66×0.254
[22]	0.13-μm SiGe	27.4	31	22.6	0.54/0.86*	2.4	>10	<–10 dB 0 to 12 GHz*	<–10 dB 45 to 67 GHz*	$2.16f_0$*	0.09×0.27
[31]	SAP	N/A	27	18.5	5.34/5.83*	2.6	>10	<–20 dB 14 to 20.5 GHz*	<–20 dB 32.5 to 50 GHz*	$1.85f_0$*	4.65×2.12×0.189
[32]	LTCC	N/A	28.7	4.5	8.65/12.2*	3	>10	<–20 dB 10 to 26.5 GHz*	<–20 dB 30.5 to 40 GHz*	$1.39f_0$*	9.7×2.2×0.42
This work	**Multi-Layer PCB**	**102/94#**	**28**	**27.9**	**21.5/7.31**	**1.3**	**>17.6**	**<–21.3 dB 0.01–22.8 GHz**	**<–24 dB 35 to 110 GHz**	**$3.92f_0$**	**1.5×1.5×0.315**

*: Obtained from the figures of measured results; IL**: insertion loss; RL***: return loss. #: $\lambda/4$ resonators and $\lambda/2$ resonator

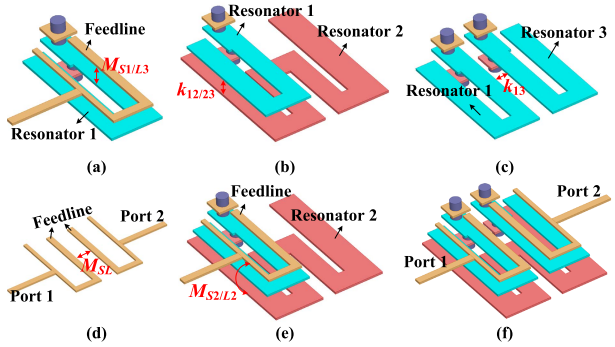

Fig. 6. (a)–(e) Coupling schemes between resonators and feed-lines. (f) Configuration of core circuit.

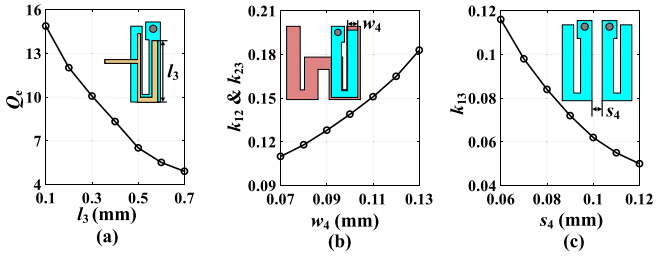

Fig. 7. (a) Influence of l_3 on the Q_e. (b) Influence of w_4 on the k_{12} and k_{23}. (c) Influence of s_4 on the k_{13}.

w_4 and s_4 can be properly adjusted to achieve a specific coupling coefficient for the passband response, as shown in Fig. 7(b) and (c).

III. MEASUREMENT

Based on proposed principles, a compact packaged mm-wave BPF based on multilayer PCB technology is fabricated. The photographs and 3-D-view configuration are shown in Fig. 8. The measurement is performed by the Agilent N5244A PNA-X microwave network analyzer (i.e., including external mm-wave converters) from 10 MHz to 110 GHz and the short-open-load-thru (SOLT) calibration is used for measurement. The measured center frequency of the BPF is 28 GHz with 3-dB fractional bandwidth (FBW) of 27.9% and minimum passband insertion loss of 1.3 dB. Meanwhile, the largest insertion loss from 24.25 to 29.5 GHz is only 2.5 dB

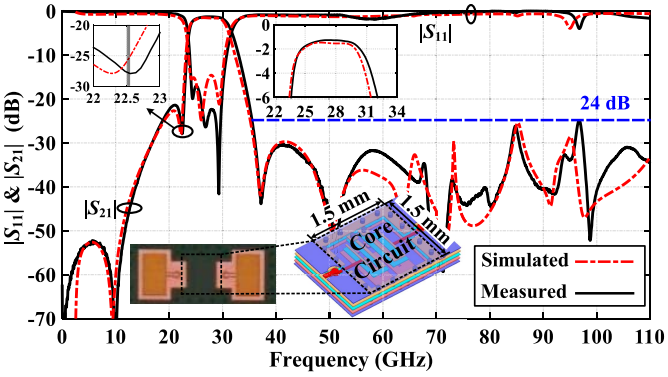

Fig. 8. Photographs of proposed filter and its simulated and measured results ($w_1 = 0.05$, $w_2 = 0.03$, $w_3 = 0.05$, $w_4 = 0.13$, $w_5 = 0.12$, $w_6 = 0.18$, $w_7 = 0.125$, $w_8 = 0.34$, $l_1 = 0.67$, $l_2 = 0.235$, $l_3 = 0.705$, $l_4 = 0.675$, $l_5 = 0.115$, $l_6 = 0.645$, $l_7 = 0.64$, $l_8 = 0.15$, $l_9 = 0.965$, $s_1 = 0.155$, $s_2 = 0.27$, $s_3 = 0.065$, $s_4 = 0.09$, $s_5 = 0.045$, and $s_6 = 0.09$, unit: mm).

(i.e., @24.25 GHz). More than 27.6 dB stopband suppression is achieved for this design from 22.5 to 22.55 GHz, while 24 dB suppression level from 35 to 110 GHz is obtained. The measured insertion loss is slightly smaller than the simulation results at the passband, since the simulation results are obtained by substrate loss tangent at 60 GHz (i.e., the substrate loss tangent is lower than 0.013 around 28 GHz). A comparison of the proposed BPF with state-of-the-arts is shown in Table I, which reveals that this BPF has merits of low insertion loss, compact size, and multi transmission zeros. Besides, this BPF can significantly improve stopband suppression without increasing the overall circuit size.

IV. CONCLUSION

In this letter, a compact packaged mm-wave BPF based on multilayer PCB technology is presented. Three controllable transmission zeros are allocated by proposed coupling topology. To reduce the circuit size and extend stopband bandwidth, three U-shape SIRs with stacked up coupling scheme are used. The measured results show that the fabricated BPF has the merits of low insertion loss, wide stopband, and high selectivity. With such good performance, the proposed BPF is attractive for 5G mm-wave applications.

REFERENCES

[1] C.-F. Chen, T.-Y. Huang, and R.-B. Wu, "Design of microstrip bandpass filters with multiorder spurious-mode suppression," *IEEE Trans. Microw. Theory Techn.*, vol. 53, no. 12, pp. 3788–3793, Dec. 2005.

[2] J.-T. Kuo, W.-H. Hsu, and W.-T. Huang, "Parallel coupled microstrip filters with suppression of harmonic response," *IEEE Microw. Wireless Compon. Lett.*, vol. 12, no. 10, pp. 383–385, Oct. 2002.

[3] P. Cheong, S.-W. Fok, and K.-W. Tam, "Miniaturized parallel coupled-line bandpass filter with spurious-response suppression," *IEEE Trans. Microw. Theory Techn.*, vol. 53, no. 5, pp. 1810–1816, May 2005.

[4] J.-K. Lee and Y.-S. Kim, "Ultra-wideband bandpass filter with improved upper stopband performance using defected ground structure," *IEEE Microw. Wireless Compon. Lett.*, vol. 20, no. 6, pp. 316–318, Jun. 2010.

[5] J.-S. Park, J.-S. Yun, and D. Ahn, "A design of the novel coupled-line bandpass filter using defected ground structure with wide stopband performance," *IEEE Trans. Microw. Theory Techn.*, vol. 50, no. 9, pp. 2037–2043, Sep. 2002.

[6] X. Luo, J.-G. Ma, E.-P. Li, and K. Ma, "Hybrid microstrip T-stub/defected ground structure cell for electromagnetic interference bandpass filter design," *IEEE Trans. Electromagn. Compat.*, vol. 53, no. 3, pp. 717–725, Aug. 2011.

[7] X. Luo, J.-G. Ma, and E.-P. Li, "Hybrid microstrip/DGS cell for filter design," *IEEE Microw. Wireless Compon. Lett.*, vol. 21, no. 10, pp. 528–530, Oct. 2011.

[8] D. Tang, C. Han, Z. Deng, H. J. Qian, and X. Luo, "Substrate-integrated defected ground structure for single and dual-band bandpass filters with wide stopband and low radiation loss," *IEEE Trans. Microw. Theory Techn.*, vol. 69, no. 1, pp. 659–670, Jan. 2021.

[9] J. Zhou, Y. Rao, D. Yang, H. J. Qian, and X. Luo, "Compact wideband BPF with wide stopband using substrate integrated defected ground structure," *IEEE Microw. Wireless Compon. Lett.*, vol. 31, no. 4, pp. 353–356, Apr. 2021.

[10] C. Han, D. Tang, Z. Deng, H. J. Qian, and X. Luo, "Filtering power divider with ultrawide stopband and wideband low radiation loss using substrate integrated defected ground structure," *IEEE Microw. Wireless Compon. Lett.*, vol. 31, no. 2, pp. 113–116, Feb. 2021.

[11] J. Xie, D. Tang, Y. Shu, and X. Luo, "Compact UWB BPF with broad stopband based on loaded-stub and C-shape SIDGS resonators," *IEEE Microw. Wireless Compon. Lett.*, early access, Dec. 31, 2021, doi: 10.1109/LMWC.2021.3136561.

[12] X. Gong *et al.*, "Precision fabrication techniques and analysis on high-Q evanescent-mode resonators and filters of different geometries," *IEEE Trans. Microw. Theory Techn.*, vol. 52, no. 11, pp. 2557–2566, Nov. 2004.

[13] G. P. Quijano, G. J. Carchon, B. K. J. C. Nauwelaers, and W. D. Raedt, "Horizontal integration of cavity filters on high-resistivity silicon thin-film technology," *IEEE Trans. Microw. Theory Techn.*, vol. 56, no. 12, pp. 2893–2901, Dec. 2008.

[14] T. R. Jones, N. Vahabisani, E. T. Der, and M. Daneshmand, "Monolithic millimeter-wave air-filled waveguide resonator for filter applications," *IEEE Microw. Wireless Compon. Lett.*, vol. 29, no. 6, pp. 379–381, Jun. 2019.

[15] A. del Olmo-Olmeda *et al.*, "A novel band-pass filter topology for millimeter-wave applications based on the groove gap waveguide," in *IEEE MTT-S Int. Microw. Symp. Dig.*, Jun. 2013, pp. 1–4.

[16] H. Kojima *et al.*, "Compact 28 GHz bandpass filter using quartz folded waveguide," in *IEEE MTT-S Int. Microw. Symp. Dig.*, Jun. 2018, pp. 1110–1113.

[17] F. Mira, J. Mateu, S. Cogollos, and V. E. Boria, "Design of ultra-wideband substrate integrated waveguide (SIW) filters in zigzag topology," *IEEE Microw. Wireless Compon. Lett.*, vol. 19, no. 5, pp. 281–283, May 2009.

[18] X.-C. Zhu *et al.*, "Design and implementation of a triple-mode planar filter," *IEEE Microw. Wireless Compon. Lett.*, vol. 23, no. 5, pp. 243–245, May 2013.

[19] Z.-C. Hao, W.-Q. Ding, and W. Hong, "Developing low-cost W-band SIW bandpass filters using the commercially available printed-circuit-board technology," *IEEE Trans. Microw. Theory Techn.*, vol. 64, no. 6, pp. 1775–1786, Jun. 2016.

[20] S. W. Wong, K. Wang, Z.-N. Chen, and Q.-X. Chu, "Design of millimeter-wave bandpass filter using electric coupling of substrate integrated waveguide (SIW)," *IEEE Microw. Wireless Compon. Lett.*, vol. 24, no. 1, pp. 26–28, Jan. 2014.

[21] D. L. Diedhiou, E. Rius, J. F. Favennec, and A. E. Mostrah, "Ku-band cross-coupled ceramic SIW filter using a novel electric cross-coupling," *IEEE Microw. Wireless Compon. Lett.*, vol. 25, no. 2, pp. 109–111, Feb. 2015.

[22] S. Chakraborty *et al.*, "A broadside-coupled meander-line resonator in 0.13-μm SiGe technology for millimeter-wave application," *IEEE Electron Device Lett.*, vol. 37, no. 3, pp. 329–332, Mar. 2016.

[23] D.-M. Kim, B.-W. Min, and J.-M. Yook, "Compact mm-wave bandpass filters using silicon integrated passive device technology," *IEEE Microw. Wireless Compon. Lett.*, vol. 29, no. 10, pp. 638–640, Oct. 2019.

[24] F. Sun, H. Zhu, X. Zhu, Y. Yang, and R. Gómez-García, "Design of on-chip millimeter-wave bandpass filters using multilayer patterned-ground element in 0.13-μm (Bi)-CMOS technology," *IEEE Trans. Microw. Theory Techn.*, vol. 67, no. 12, pp. 5159–5170, Dec. 2019.

[25] C.-Y. Hsu, C.-Y. Chen, and H.-R. Chuang, "70 GHz folded loop dual-mode bandpass filter fabricated using 0.18 μm standard CMOS technology," *IEEE Microw. Wireless Compon. Lett.*, vol. 18, no. 9, pp. 587–589, Sep. 2008.

[26] B. Dehlink, M. Engl, K. Aufinger, and H. Knapp, "Integrated bandpass filter at 77 GHz in SiGe technology," *IEEE Microw. Wireless Compon. Lett.*, vol. 17, no. 5, pp. 346–348, May 2007.

[27] K. Y. Chan, R. Ramer, R. R. Mansour, and Y. J. Guo, "60 GHz to E-band switchable bandpass filter," *IEEE Microw. Wireless Compon. Lett.*, vol. 24, no. 8, pp. 545–547, Aug. 2014.

[28] H. Zhu, Y. Yang, X. Zhu, Y. Sun, and S.-W. Wong, "Miniaturized resonator and bandpass filter for silicon-based monolithic microwave and millimeter-wave integrated circuits," *IEEE Trans. Circuits Syst. I, Reg. Papers*, vol. 65, no. 12, pp. 4062–4071, Dec. 2018.

[29] V. N. R. Vanukuru and V. K. Velidi, "CMOS millimeter-wave ultra-wideband bandpass filter with three reflection-zeros using compact single TFMS coupled-line hairpin unit," *IEEE Trans. Circuits Syst. II, Exp. Briefs*, vol. 67, no. 1, pp. 77–81, Jan. 2020.

[30] L. Nan, K. Mouthaan, Y. Z. Xiong, J. Shi, S. C. Rustagi, and B. L. Ooi, "Design of 60- and 77-GHz narrow-bandpass filters in CMOS technology," *IEEE Trans. Circuits Syst. II, Exp. Briefs*, vol. 55, no. 8, pp. 738–742, Aug. 2008.

[31] M. Ali *et al.*, "First demonstration of compact, ultra-thin low-pass and bandpass filters for 5G small-cell applications," *IEEE Microw. Wireless Compon. Lett.*, vol. 28, no. 12, pp. 1110–1112, Dec. 2018.

[32] B. G. Choi, M. G. Stubbs, and C. S. Park, "A Ka-band narrow bandpass filter using LTCC technology," *IEEE Microw. Wireless Compon. Lett.*, vol. 13, no. 9, pp. 388–390, Sep. 2003.

[33] J.-H. Lee *et al.*, "Highly integrated millimeter-wave passive components using 3-D LTCC system-on-package (SOP) technology," *IEEE Trans. Microw. Theory Techn.*, vol. 53, no. 6, pp. 2220–2229, Jun. 2005.

[34] L. Rigaudeau *et al.*, "LTCC 3-D resonators applied to the design of very compact filters for Q-band applications," *IEEE Trans. Microw. Theory Techn.*, vol. 54, no. 6, pp. 2620–2627, Jun. 2006.

[35] J. H. Lee, S. Pinel, J. Laskar, and M. M. Tentzeris, "Design and development of advanced cavity-based dual-mode filters using low-temperature co-fired ceramic technology for V-band gigabit wireless systems," *IEEE Trans. Microw. Theory Techn.*, vol. 55, no. 9, pp. 1869–1879, Sep. 2007.

[36] Y. Shi, W. Feng, H. Wang, S. Zheng, M. Zhou, and Q. Wu, "Compact planar W-band front-end module based on EBG packaging and LTCC circuits," *IEEE Trans. Circuits Syst. II, Exp. Briefs*, vol. 68, no. 3, pp. 878–882, Mar. 2021.

[37] X. Luo, B. Yang, and H. J. Qian, "Adaptive synthesis for resonator-coupled filters based on particle swarm optimization," *IEEE Trans. Microw. Theory Techn.*, vol. 67, no. 2, pp. 712–725, Feb. 2019.

[38] (2021). *Radiocommunication Sector of ITU*. [Online]. Available: https://www.itu.int/en/publications/ITU-R

[39] S.-C. Lin, P.-H. Deng, Y.-S. Lin, C.-H. Wang, and C. Hsiung Chen, "Wide-stopband microstrip bandpass filters using dissimilar quarter-wavelength stepped-impedance resonators," *IEEE Trans. Microw. Theory Techn.*, vol. 54, no. 3, pp. 1011–1018, Mar. 2006.

[40] J.-S. Hong, *Microwave Filter for RF/Microwave Application*. New York, NY, USA: Wiley, 2011.